Commercial Synthetic Aperture Radar Data for Surface Deformation and Change

Stacey Huang[1,2], Batuhan Osmanoglu[2], MinJeong Jo[1,2], Bernd Scheuchl[3], Enrico Ciraci[3]

[1]University of Maryland, Baltimore County, [2]Goddard Space Flight Center, NASA,
[3]Department of Earth System Science, University of California, Irvine

Abstract

The commercial synthetic aperture radar (SAR) market is experiencing year-over-year growth and is currently capable of imaging anywhere in the world within an hour at X-band. Surface Deformation and Change (SDC) is a mission study at NASA to investigate innovative architectures beyond the NASA-ISRO SAR (NISAR) mission in the next decade. In this article we present preliminary findings on the technical capabilities of the currently available commercial SAR data, and investigate their applicability to SDC goals, such as imaging quality and retrieval of surface motion.

***Index Terms*—** SAR, NISAR, SDC, InSAR

1. INTRODUCTION

The SDC study team analyzed currently available commercial constellations and the SAR data generated by these constellations. Here, we specifically assessed data from Capella Space and ICEYE constellations. Assessments mainly focused on impulse response functions over corner reflectors in Rosamond, CA as well as interferometric quality over several sites across the globe.

Although we are reporting our results from only two Smallsat-led commercial data providers in this effort, with one comparison included to an agency-led commercial company, the SDC team has analyzed the commercial SAR market capability as a whole through their published characteristics [1]. Therefore, the discussions presented in this paper address commercial providers as a whole instead of the vendors from which we have obtained data.

2. DATA

We evaluated a variety of SAR data products over a diverse set of terrain from both Capella Space and ICEYE (Table I). Other than Rosamond, the remaining AOIs were contingent on scene availability from providers; Capella interferometry products are currently only available on an opportunistic basis, while ICEYE can deliver ground track repeat imagery from a small number of dedicated satellites. We processed data using both the GAMMA software [2] and the Stanford InSAR System [3]. We used the Copernicus DEM [4] for topographic correction and geocoding.

Table 1. Imagery utilized in the study.

Provider	Mode	AOI*	Qty	Date Range
Capella	Strip	RMUS	1	2022/12/18
Capella	Spot	RMUS	2	2021/08-2022/12
Capella	Spot	WAAU	6	2021/07-2021/09
Capella	Spot	PYNK	2	2023/04/22-2023/04/28
Capella	Spot	SUTR	2	2023/05/11-2023/05/24
Capella	Spot	KAIR	8	2022/07-2023/02
ICEYE	Strip	RMUS	14	2022/07/19-2022/09/05
ICEYE	Strip	PGGL	4**	2021/10/26-2021/10/29

* RMUS=Rosamond, CA, USA; WAAU=West Angelas Mine, Australia; PYNK=Pyonygang, North Korea; SUTR=Şanlıurfa, Türkiye; KAIR=Kashan Airport, Iran; PGGL=Petermann Glacier, Greenland
** Example from [5] which used a larger data set

3. IMPULSE RESPONSE FUNCTION (IRF)

We analyzed the IRF of 23 corner reflectors with a 2.4 m side length in ICEYE X-7 imagery, in terms of Peak Sidelobe Ratio (PSLR), Integrated Sidelobe Ratio (ISLR), -3 dB width spatial resolution, and geolocation accuracy. A stack of 14 stripmap images was obtained over the Rosamond calibration site in California. Fig. 1 shows the mean and standard deviations of each parameter. -3 dB resolutions are ~1.25 and ~2.76 m in range and azimuth directions, respectively, while the expected resolutions for range and azimuth are 1.5 m and 2.5-3.0 m, respectively [6]. Corner reflector locations were compared with their positions in the ICEYE images. Geolocation accuracy in the range direction falls within the expected values of 3.2 m [7], while the location errors in the azimuth direction are close to the expected. The PSLR and ISLR were also all within or slightly worse than the values provided in the ICEYE documentation.

We also analyzed one Stripmap (SM) and two Spotlight (SP) mode Capella imagery over the Rosamond site. Table 2 lists the IRF analysis results of the average and standard deviation of all included corner reflectors. The range and azimuth resolutions of SM mode data are 0.67 and 1.19 m, respectively, which are within the expected values of 0.75 and 1.2 m provided in the Capella documentation [8]. For the SP mode data, the azimuth resolutions in both images are within the expected value of 0.5 m. The range resolutions in both images are 0.38 and 0.28 m, falling within and slightly exceeding the expected value of 0.3 m.

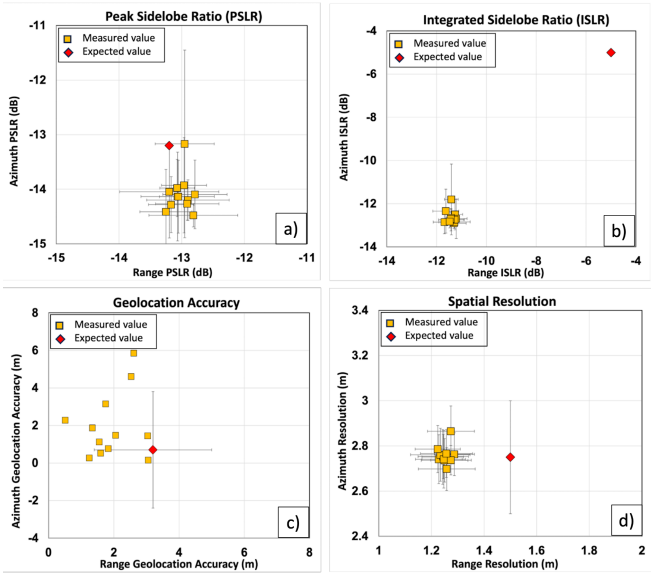

Figure 1. Assessment of the ICEYE IRF of corner reflectors over Rosamond, CA: a) PSLR, b) ISLR, c) Geolocation, d) Resolution. Expected values can be found in [4], [5].

For range spectra processing, the 2021 SP imagery used an exponential window with parameter α=1.25, resulting in a PSLR of about -24 dB and ISLR of about -25 dB, while the 2022 imagery used a rectangular window, resulting in a PSLR and ISLR of about -11 dB. Similar levels of geolocation accuracy were measured using both the SM and SP mode imagery, with approximately 2.5 m or less error in the range direction and approximately 0.18 or less error in the azimuth direction.

Table 2. Rosamond IRF analysis for Capella SM/SP mode images.

	SM_20221218	SP_20210812	SP_20221231
Range Res. [m]	0.67±0.04	0.381±0.04	0.28±0.04
Azimuth Res. [m]	1.19±0.07	0.44±0.06	0.47±0.07
Range PSLR [dB]	-13.41±0.19	-24.39±0.22	-11.41±1.54
Azimuth PSLR [dB]	-17.58±0.15	-13.27±0.20	-12.69±0.85
Range ISLR [dB]	-11.57±0.14	-25.05±0.54	-11.77±1.58
Azi. ISLR [dB]	-16.45±0.13	-12.00±0.15	-11.41±0.60
Rg. Loc. Acc. [m]	2.53±1.10	2.25±0.62	2.52±0.04
Az. Loc. Acc. [m]	0.18±0.22	0.13±0.08	0.13±0.04

4. SPATIAL DECORRELATION ANALYSIS

Correlation is one of the most important measures of data quality in interferometry. Decorrelation can result from a variety of factors, from sensor and spacecraft-based factors to the types of imaged terrain. We characterized trends of average spatial decorrelation in several interferometric pairs over a variety of terrain types and compared to theoretically computed values. The equation for spatial decorrelation $\rho_{spatial}$ is given by Zebker and Villasenor [9]:

$$\rho_{spatial} = 1 - \frac{2|B|R_y cos^2\theta}{\lambda r} \quad (1)$$

where B is the perpendicular baseline, R_y is the range resolution, θ is the look angle, λ is the sensor wavelength, and r is the range. The equation for the critical baseline B_c is then obtained by solving for $\rho_{spatial} = 0$:

$$B_c = \frac{\lambda r}{2R_y cos^2\theta} \quad (2)$$

The critical baselines over a flat terrain for several commercial vendors are summarized in Table 3, using published spotlight range resolution and a look angle of 30 degrees. The satellite range is calculated based on advertised orbit altitudes (H), such that $r = H/cos(\theta)$. We found a discrepancy between observed average coherence values and their theoretically predicted values in the case studies are highlighted in the following subsections.

4.1. West Angelas Mine, Australia (Capella)

We processed a set of 6 spotlight SLCs from Capella over the main dig site of West Angelas mine, an iron mine in western Australia. Using (2), we calculated a critical baseline for this dataset of about 35 km; parameters differed slightly from the values listed in Table 2, most notably that range resolution was 0.5 m rather than 0.3 m. 12 interferograms had baselines less than 30 km and should have been viable. In practice, only 4 interferograms were coherent, all with baselines less than 10 km. The two interferograms with the shortest baselines, along with their coherence plots, are shown in Fig. 2. Interferogram fringes in Fig. 2 can likely be attributed to elevation changes relative to the Copernicus DEM due to mining activity. Even at a baseline of 5 km (Fig. 3d), which is ⅛ of the theoretical limit, the coherence has rapidly dropped. Coherence drops rapidly with a perpendicular baseline across all 12 interferograms (Fig. 3).

4.2. Urban areas (Capella)

We studied data from three urban areas: 1) Pyongyang, North Korea; 2) Şanlıurfa, Türkiye; and 3) Kashan Airport, Iran. We observed significant orbital ramps in all interferograms.To deramp the images, we fitted and subtracted a polynomial surface for each individual interferogram.A sample of original and corrected interferograms, along with their associated coherence maps, are shown in Fig. 4.

Table 3. Critical baselines for each vendor as computed from (2).

Provider	R_y (m)	θ (deg)	λ (cm)	H (km)	B (m)
Capella	0.3	30	3.11	525.0	41,880
ICEYE	0.5	30	3.11	570.0	27,282
Umbra	0.15	30	3.06	527.5	82,271

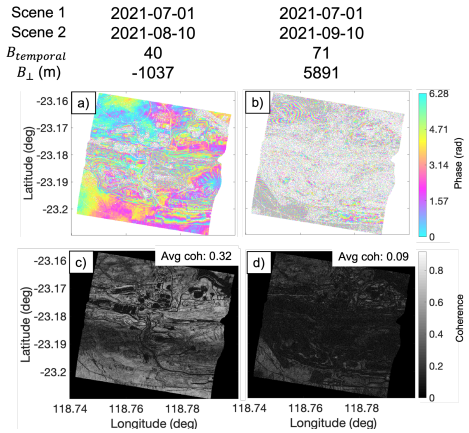

Figure 2. West Angelas Mine interferograms with the shortest baselines (a,b) and their corresponding coherence plots (c,d).

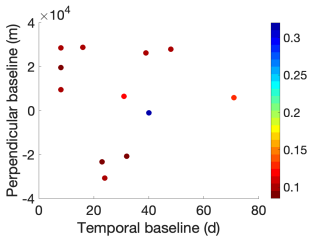

Figure 3. Average coherence, signified by dot colors, with temporal and perpendicular baseline plot for interferograms over West Angelas Mine, Australia.

As with West Angelas Mine, a similar drop in coherence with perpendicular baseline is observed (Fig. 5a). With the larger range of spatial baselines with this dataset, we can also plot the observed vs. theoretical coherence with baseline (Fig. 5b), with theoretical trends calculated from (1). The observed values start much lower than 1 and also plateau at a value higher than 0 (in this case, about 0.06), which reflects the well-known phenomenon of overestimation of empirical coherence values.

4.3. Comparison with COSMO-SkyMed (CSK)

COSMO-SkyMed (CSK) is another commercial satellite constellation also operating at X-band since 2007 that is owned and operated by ASI (Agenzia Spaziale Italiana). Thus, it is a useful data source to compare with New Space commercially available products. We analyzed publicly available H-IMAGE data over the Kilauea Supersite. We chose an AOI over the volcano of about 25 x 25 km containing a mix of open-faced lava flows (very coherent) to vegetation (very incoherent).

We found that the correlation drop with spatial baseline was low compared to Capella (Fig. 6). The marked differences in trends between CSK and Capella data are clear, in particular that: 1) the average starting coherence values are much higher; and 2) the drop in coherence with baseline is much less significant, although the critical baseline is smaller (~6 km).

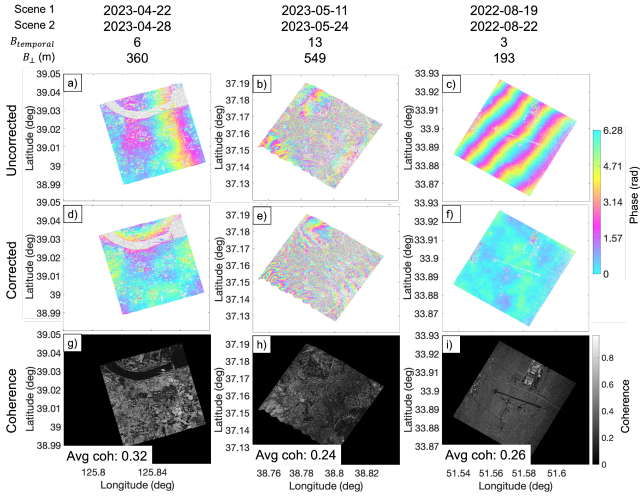

Figure 4. Uncorrected (a-c) and corrected (d-f) interferograms from urban analysis and the corresponding coherence (g-i). Analyzed areas include North Korea (a, d, g); Türkiye (b, e, h), and Iran (c, g, i).

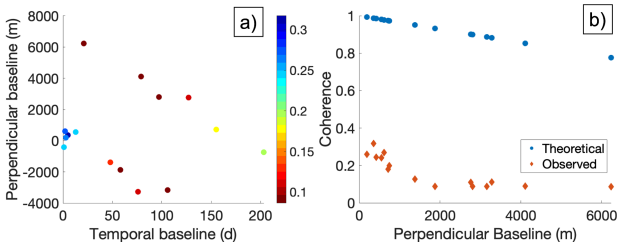

Figure 5. a) Average coherence with temporal and perpendicular baseline for interferograms over all urban areas; b) observed and theoretical average coherence with perpendicular baseline.

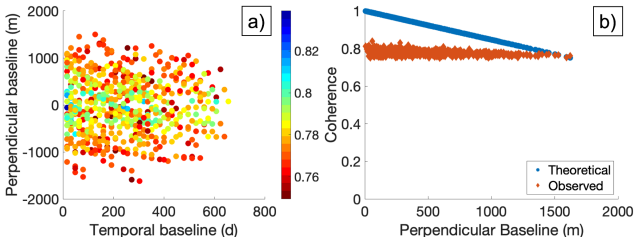

Figure 6. Same plots as Fig. 5, but for CSK interferograms over Kilauea volcano (note that colors for a) are rescaled for contrast and span a different range than Figs. 3 and 5).

5. INSAR FOR GLACIER APPLICATIONS

SAR interferometry proves particularly useful for ice sheet science with a number of international projects generating geophysical information products like ice velocity and grounding line location maps based on data from international SAR missions.Strategic coverage of these regions with high spatial and temporal resolution time series would be a desirable addition to the program of record.

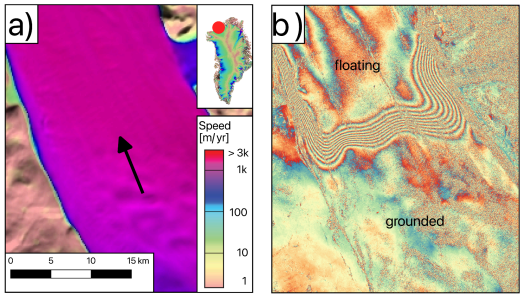

Figure 7. a) Velocity map of Petermann Glacier NW Greenland (see inset). Arrow indicates flow direction; b) ICEYE double difference interferogram (2021 10/26-10/27 & 10/28-10/29) indicates the boundary between grounded and floating ice. The dense fringes indicate flexing ice, the upstream edge is the grounding line.

While several commercial vendors are working towards InSAR capability, we had access to ICEYE data only for the purpose of this study. The capability of ICEYE to collect data on a daily basis with a repeat orbit (albeit with some restriction on coverage, baselines, and time series duration, at the time of submission) made it an ideal candidate to test grounding line measurements using a short repeat data set. The concept has been proven in an independent study for Petermann Glacier in Northern Greenland [5] and additional research is underway for other test sites. Fig. 7 shows an example double difference interferogram of Petermann glacier in Greenland. The resulting phase pattern shows vertical deformation of the glacier due to different tide states at the times of acquisitions. A dense fringe pattern indicates the bending of the ice where it lifts off the ground and starts to float in the ocean. The upstream boundary of the fringe band is the grounding line. With multiple scenes acquired over several days, several grounding line measurements can be made to evaluate the short term migration of the grounding line due to tide. This variation is also referred to as the ice grounding zone. The fact that the orbit control of ICEYE at the time of data acquisition was limited and mostly next-neighbor interferograms worked, as opposed for the entire stack, had no impact for this application as differences of next neighbor interferograms are the basis for grounding line measurements.

6. DISCUSSION

PSLR and ISLR values for a SAR image depends on several factors including knowledge of antenna position, matched filtering and windowing function applied during image focusing. As seen in Fig. 1(a-b), all of the analyzed responses in ICEYE imagery are within the expected range, considering the standard deviation of all included corner reflectors in a scene. While Capella does not provide information on the expected side lobe levels, the measured PSLR values are slightly above theoretical values given applied windowing filters.

Currently, the rapid drop in the observed correlation with spatial baseline vs. the theoretical trend will reduce the potential availability of usable scenes that can meet SDC goals, and performance seems to be lower than that of comparable sensors such as CSK. However, continued improvements to provider data processing and end-user software may enable interferogram viability with baselines closer to theoretically predicted. As noted in [9], non-ideal characteristics of various elements in the radar as well as windowing used during the processing may alter the decorrelation function in (1) and the resulting critical baseline derived in (2).

Glacier applications can greatly benefit from strategically placed observations in key areas where agency based missions to date do not provide sufficient information due to decorrelation as a function of long revisit in combination with high glacier speed. The key advantage of the ICEYE constellation is the capability to collect data stacks at high frequency (i.e. daily) repeat. It should be noted orbit control at the time of data collection was not so stringent as to keep the orbital tube small enough to satisfy interferometric conditions for the entire stack collected, however, next neighbor interferograms generally worked, which fit the requirement for grounding line measurements. This aspect is expected to improve for later generation satellites and will make future data stacks collected more suitable for a larger variety of InSAR applications.

Combined with [1], these results give a better picture of applications for which commercial SAR data will be able to contribute to SDC's needs. For example, interferometric capability is required for more than half the SDC observables, while just under half of the observables benefit from 3-day or faster revisit. Therefore, it may be possible to augment a future SDC mission architecture with commercial data to provide rapid-revisit in targeted areas.

7. CONCLUSION

In this paper, we have studied the technical capabilities of X-band commercial data with a focus on the SDC mission. Our analysis indicates that the provided imagery is within spec in terms of spatial resolution, geolocation accuracy and demonstrates reasonable PSLR and ISLR characteristics. The relevance of commercial imagery to a future SDC mission can be increased through improved orbit control and increased availability of interferometry with higher coherence. Unique applications such as daily glacial observations present opportunities to advance scientific understanding with current commercial capabilities.

8. REFERENCES

[1] B. Osmanoglu *et al.*, "BENEFIT ASSESSMENT OF COMMERCIAL SYNTHETIC APERTURE RADAR OBSERVATIONS FOR NASA'S SURFACE DEFORMATION AND CHANGE MISSION STUDY," in *39th International Symposium on Remote Sensing of*

Environment (ISRSE-39) "From Human needs to SDGs" - 24–28 April 2023, Antalya, Türkiye, Copernicus GmbH, Apr. 2023, pp. 225–232.

[2] U. Wegnüller, C. Werner, T. Strozzi, A. Wiesmann, O. Frey, and M. Santoro, "Sentinel-1 Support in the GAMMA Software," *Procedia Comput. Sci.*, vol. 100, pp. 1305–1312, Jan. 2016.

[3] H. A. Zebker, "Sentinel-1 analysis ready data - A convenient and easy to use system producing common-coordinate timeseries," *AGUFM*, vol. 2022, p. G42D–0257, 2022.

[4] E. Fahrland, P. Jacob, H. Schrader, and H. Kahabka, "Copernicus Digital Elevation Model Product Handbook," Airbus Defence and Space GmbH, GEO.2018-1988-2, Jun. 2020. [Online]. Available: https://spacedata.copernicus.eu/documents/20126/0/GEO1988-CopernicusDEM-SPE-002_ProductHandbook_I1.00.pdf

[5] E. Ciracì *et al.*, "Melt rates in the kilometer-size grounding zone of Petermann Glacier, Greenland, before and during a retreat," *Proc. Natl. Acad. Sci. U. S. A.*, vol. 120, no. 20, p. e2220924120, May 2023.

[6] V. Ignatenko, P. Laurila, A. Radius, L. Lamentowski, O. Antropov, and D. Muff, "ICEYE Microsatellite SAR Constellation Status Update: Evaluation of First Commercial Imaging Modes," in *IGARSS 2020 - 2020 IEEE International Geoscience and Remote Sensing Symposium*, IEEE, Sep. 2020, pp. 3581–3584.

[7] "Validation - ICEYE Product Documentation." https://sar.iceye.com/5.1.2/foundations/validation/geospatialValidation/ (accessed Jan. 11, 2024).

[8] Capella Space, "Capella Space SAR Imagery Products Guide," Capella Space, 3.9, Dec. 2023. [Online]. Available: https://support.capellaspace.com/hc/en-us/article_attachments/21587738168340

[9] H. A. Zebker and J. Villasenor, "Decorrelation in Interferometric Radar Echoes," *IEEE Trans. Geosci. Remote Sens.*, vol. 30, pp. 950–959, Sep. 1992.